

# Oncogenic 3D genome conformations identify novel therapeutic targets in ependymoma

**Konstantin Okonechnikov**

Hopp Children's Cancer Center (KITZ)

**Aylin Camgoz**

Hopp Children's Cancer Center (KITZ)

**Donglim Esther Park**

UCSD

**Owen Chapman**

UCSD

**Jens-Martin Hübner**

Hopp Children's Cancer Center (KITZ)

**Abhijit Chakraborty**

La Jolla Institute for Immunology

**Meghana Pagadala**

UCSD

**Rosalind Bump**

Salk Institute for Biological Studies

**Sahaana Chandran**

Salk Institute for Biological Studies

**Katerina Kraft**

Stanford University

**Rocio Acuna-Hidalgo**

10. Max Planck Institute for Molecular Genetics

**Derek Reid**

Arima Genomics, Inc

**Edwin F. Juarez**

UCSD

**James T. Robinson**

UCSD

**Kristian W. Pajtler**

German Cancer Research Center

**Monika Mauermann**

Hopp Children's Cancer Center NCT Heidelberg (KITZ)

**Till Milde**

German Cancer Research Center (DKFZ) <https://orcid.org/0000-0002-7267-1052>

**Nicole G. Coufal**

UCSD

**Michael Levy**

Rady Children's Hospital-San Diego

**Denise Malicki**

Rady Children's Hospital

**Shareef Nahas**

Rady Children's Hospital

**Matija Snuderl**

NYU Langone Health

**John Crawford**

Rady Children's Hospital

**Robert J. Wechsler-Reya**

Sanford Burnham Prebys Medical Discovery Institute <https://orcid.org/0000-0002-7463-8352>

**Stefan Mundlos**

Max Planck Institute for Molecular Genetics <https://orcid.org/0000-0002-9788-3166>

**Anthony Schmitt**

Arima Genomics

**Hannah Carter**

UCSD

**Kulandaimanuel Antony Michaelraj**

Hospital for Sick Children

**Sachin A. Kumar**

The Hospital for Sick Children <https://orcid.org/0000-0002-4853-3864>

**Michael D. Taylor**

Sickkids Hospital

**Jeremy Rich**

Division of Regenerative Medicine, Department of Medicine, University of California San Diego

**Frank Buchholz**

TU Dresden

**Jill P. Mesirov**

University of California, San Diego

**Stefan M. Pfister**

Division of Pediatric Neurooncology, German Cancer Research Center (DKFZ)

**Ferhat Ay**

La Jolla Institute For Immunology <https://orcid.org/0000-0002-0708-6914>

**Jesse R. Dixon**

Salk Institute for Biological Studies <https://orcid.org/0000-0002-6273-2181>

**Marcel Kool**

Division of Pediatric Neuro-oncology and German Cancer Consortium (DKTK), German Cancer Research Center (DKFZ), Heidelberg

**Lukas Chavez** (✉ [lukaschavez@health.ucsd.edu](mailto:lukaschavez@health.ucsd.edu))

University of California, San Diego

---

## Biological Sciences - Article

**Keywords:** ependymoma, tumorigenesis, oncogenic mechanisms

**Posted Date:** November 5th, 2020

**DOI:** <https://doi.org/10.21203/rs.3.rs-88331/v1>

**License:**   This work is licensed under a Creative Commons Attribution 4.0 International License.

[Read Full License](#)

---

1 ***Oncogenic 3D genome conformations identify novel therapeutic targets in***  
2 ***ependymoma.***

3  
4 Konstantin Okonechnikov<sup>1,2,\*</sup>, Aylin Camgoz<sup>1,2,3,\*</sup>, Donglim Esther Park<sup>4,5</sup>, Owen Chapman<sup>6</sup>, Jens-  
5 Martin Hübner<sup>1,2</sup>, Abhijit Chakraborty<sup>7</sup>, Meghana Pagadala<sup>6</sup>, Rosalind Bump<sup>8</sup>, Sahaana Chandran<sup>8</sup>,  
6 Katerina Kraft<sup>9</sup>, Rocio Acuna-Hidalgo<sup>10,11</sup>, Derek Reid<sup>12</sup>, Edwin F. Juarez<sup>6</sup>, James T. Robinson<sup>6</sup>,  
7 Kristian W. Pajtler<sup>1,2,13</sup>, Monika Mauermann<sup>1,2</sup>, Till Milde<sup>1,13,14</sup>, Nicole G. Coufal<sup>15,18</sup>, Michael  
8 Levy<sup>16</sup>, Denise Malicki<sup>17</sup>, Shareef Nahas<sup>18</sup>, Matija Snuderl<sup>19,20</sup>, John Crawford<sup>21</sup>,  
9 Robert J. Wechsler-Reya<sup>5,14,22</sup>, Stefan Mundlos<sup>10</sup>, Anthony Schmitt<sup>12</sup>, Hannah Carter<sup>6</sup>,  
10 Kulandaimanuel Antony Michealraj<sup>23</sup>, Sachin A. Kumar<sup>23</sup>, Michael D. Taylor<sup>23</sup>, Jeremy Rich<sup>4,5,24</sup>,  
11 Frank Buchholz<sup>3,25,26</sup>, Jill P. Mesirov<sup>6,27</sup>, Stefan M. Pfister<sup>1,2,13</sup>, Ferhat Ay<sup>7,14</sup>, Jesse R. Dixon<sup>8</sup>,  
12 Marcel Kool<sup>1,2,28,#</sup>, Lukas Chavez<sup>6,27,#,+</sup>

- 13  
14 1. Hopp Children's Cancer Center (KiTZ), Heidelberg, Germany;  
15 2. Division of Pediatric Neurooncology, German Cancer Research Center (DKFZ) and German  
16 Cancer Consortium (DKTK), Heidelberg, Germany;  
17 3. National Center for Tumor Diseases (NCT): German Cancer Research Center (DKFZ)  
18 Heidelberg, Faculty of Medicine and University Hospital Carl Gustav Carus, Technische  
19 Universität Dresden, Helmholtz-Zentrum Dresden-Rossendorf (HZDR), Dresden, Germany;  
20 4. Division of Regenerative Medicine, Department of Medicine, University of California, San  
21 Diego, La Jolla, CA 92037, USA;  
22 5. Sanford Consortium for Regenerative Medicine, 2880 Torrey Pines Scenic Drive, La Jolla,  
23 CA 92037, USA;  
24 6. Division of Medical Genetics, Department of Medicine, University of California San Diego  
25 (UCSD), San Diego, USA;  
26 7. Centers for Cancer Immunotherapy and Autoimmunity, La Jolla Institute for Immunology,  
27 La Jolla, CA, USA;  
28 8. Peptide Biology Labs, Salk Institute for Biological Studies, La Jolla, CA, USA;  
29 9. Center for Personal Dynamic Regulomes, Stanford University, Stanford, CA, USA ;  
30 10. Max Planck Institute for Molecular Genetics, Berlin, Germany;  
31 11. Institute for Medical Genetics and Human Genetics, Charité Universitätsmedizin Berlin,  
32 Berlin, Germany;  
33 12. Arima Genomics, Inc. San Diego, CA, 92121;

- 34 13. Department of Pediatric Oncology, Hematology and Immunology, Heidelberg University  
35 Hospital, Heidelberg, Germany;
- 36 14. CCU Pediatric Oncology, German Cancer Research Center (DKFZ) and German Cancer  
37 Consortium (DKTK), Heidelberg, Germany;
- 38 15. Department of Pediatrics, University of California, San Diego, San Diego, CA 92093, USA;
- 39 16. Neurosurgery, University of California San Diego – Rady Children's Hospital, San Diego,  
40 CA 92123, USA;
- 41 17. Pathology, University of California San Diego – Rady Children's Hospital, San Diego, CA  
42 92123, USA;
- 43 18. Rady Children's Institute for Genomic Medicine, San Diego, California 92123, USA;
- 44 19. Department of Pathology, NYU Langone Health, NYU Grossman School of Medicine, 550  
45 First Ave, New York, NY 10016 USA;
- 46 20. Laura and Isaac Perlmutter Cancer Center, NYU Langone Health, New York, NY USA;
- 47 21. Department of Neurosciences, University of California San Diego – Rady Children's  
48 Hospital, San Diego, CA 92123, USA;
- 49 22. Tumor Initiation and Maintenance Program, NCI-Designated Cancer Center, Sanford  
50 Burnham Prebys Medical Discovery Institute, La Jolla, CA, USA;
- 51 23. Division of Neurosurgery, Arthur and Sonia Labatt Brain Tumor Research Center, Hospital  
52 for Sick Children, University of Toronto, Toronto, Ontario, Canada;
- 53 24. Department of Neurosciences, School of Medicine, University of California San Diego, La  
54 Jolla, CA 92037, USA;
- 55 25. Medical Systems Biology, Medical Faculty and University Hospital Carl Gustav Carus, TU  
56 Dresden, 01307 Dresden, Germany;
- 57 26. German Cancer Research Center (DKFZ), Heidelberg and German Cancer Consortium  
58 (DKTK) Partner Site Dresden, Germany;
- 59 27. Moores Cancer Center, University of California San Diego (UCSD), La Jolla, CA, USA;
- 60 28. Princess Máxima Center for Pediatric Oncology, Utrecht, The Netherlands.

61 \*These authors contributed equally to this work.

62 #These authors are co-senior authors.

63 + Manuscript correspondence.

64

65

66

## 67 **Abstract**

68 Ependymoma is a tumor of the brain or spinal cord. The two most common and aggressive molecular  
69 groups of ependymoma are the supratentorial *RELA*-fusion associated group and the posterior fossa  
70 ependymoma group A. In both groups, tumors occur mainly in young children and frequently recur  
71 after treatment<sup>1</sup>. Although the molecular mechanisms underlying these diseases have recently been  
72 uncovered, they remain difficult to target and innovative therapeutic approaches are urgently needed.  
73 Here, we use genome-wide chromosome conformation capture (Hi-C), complemented with CTCF  
74 (insulators) and H3K27ac (active enhancers) ChIP-seq as well as gene expression and whole-genome  
75 DNA methylation profiling in primary and relapsed ependymoma tumors and cell lines to identify  
76 chromosomal rearrangements and regulatory mechanisms underlying aberrant expression of genes that  
77 are essential for ependymoma tumorigenesis. In particular, we observe the formation of new  
78 topologically associating domains ('neo-TADs') by intra- and inter-chromosomal structural variants,  
79 tumor-specific 3D chromatin complexes of regulatory elements, and the replacement of CTCF  
80 insulators by DNA hyper-methylation as novel oncogenic mechanisms in ependymoma. Through  
81 inhibition experiments we validated that the newly identified genes, including *RCOR2*, *ITGA6*,  
82 *LAMC1*, and *ARL4C*, are highly essential for the survival of patient-derived ependymoma models in a  
83 disease subtype-specific manner. Thus, this study identifies potential novel therapeutic vulnerabilities  
84 in ependymoma and extends our ability to reveal tumor-dependency genes and pathways by oncogenic  
85 3D genome conformations even in tumors that lack known genetic alterations.

86

## 87 **Main**

88 Tumors of the central-nervous system (CNS) are the most common cancers in children aged 0-14 years  
89 and a leading cause of death during childhood<sup>2-4</sup>. Intracranial ependymomas are segregated on the  
90 basis of anatomical location (supratentorial versus infratentorial or posterior fossa) and further divided  
91 by DNA methylation and expression profiling into distinct molecular groups that reflect differences in  
92 the age of onset, gender predominance, response to therapy, and genetic aberrations that drive the  
93 disease<sup>1,5,6</sup>. The supratentorial *RELA*-fusion associated group is characterized by recurrent complex  
94 chromothripsis events in chromosome 11 that lead to different types of *C11orf95-RELA* fusion genes,  
95 which have been shown to drive tumorigenesis in this group of tumors<sup>7,8</sup>. In contrast, initial DNA  
96 sequencing studies showed an absence of recurrent mutations or gene fusions in posterior fossa  
97 ependymoma group A (PFA), suggesting that these tumors might be epigenetically driven<sup>5,7</sup>. Indeed,  
98 global loss of histone H3 lysine 27 trimethylation (H3K27me3), a histone modification associated with  
99 the negative regulation of gene expression, was identified as a marker for PFA tumors<sup>9</sup>. Recent studies

100 have revealed that EZH inhibitory protein EZHIP (previously known as *CXorf67*), which is aberrantly  
101 expressed in most PFA ependymomas, causes downregulation of H3K27me3 by inhibiting EZH2 in  
102 the polycomb repressive complex 2 (PRC2)<sup>10,11</sup>. The few PFA ependymomas that do not overexpress  
103 *EZHIP* appeared to harbor K27M mutations in H3.1 or H3.3, which also inhibit EZH2. Furthermore,  
104 gain of chromosome arm 1q, present in ~25% of all PFA tumors, has been associated with a  
105 particularly poor survival of PFA patients, but the underlying driver mechanism remains unknown<sup>10,12</sup>.  
106 Since there are no small molecules available directly targeting the C11orf95-RELA fusions or EZHIP,  
107 and since it is not yet known whether EZHIP alone drives tumorigenesis in PFA, a better understanding  
108 of the tumor driving mechanisms and how they can be targeted is urgently needed. New insights into  
109 the regulation of gene expression during normal and diseased human development have recently been  
110 gained by analyzing 3D chromatin architectures<sup>13-15</sup>. Therefore, we have combined Hi-C with  
111 complementary molecular profiling techniques of ependymoma tumors and cell lines to investigate  
112 whether changes in intra- or inter- chromosomal DNA interactions in these tumors may lead to  
113 activation of specific oncogenes and may identify novel targets and tumor dependencies (**Figure 1a**).  
114

### 115 ***The 3D genome organization of ependymoma tumors***

116 We have performed Hi-C<sup>16</sup> followed by deep sequencing in 14 PFA and RELA ependymoma samples,  
117 comprising eleven tumors (fresh frozen or FFPE) and three cell lines (**Figure 1b, Suppl. Figure 1a**).  
118 Most samples were also analyzed by chromatin immunoprecipitation targeting the histone  
119 modification H3K27ac, which is associated with active chromatin, followed by sequencing (ChIP-seq,  
120 n=9), gene expression (RNA-seq, n=11), whole genome sequencing (WGS, n=12) and DNA  
121 methylation (n=14, **Suppl. Table 1**). PFA and RELA ependymoma groups can be clearly distinguished  
122 using various molecular profiling techniques including DNA methylation<sup>17</sup> (**Suppl. Figure 1b**).  
123 Unsupervised clustering of the Hi-C data also clusters ependymoma tumors into the expected groups,  
124 demonstrating pronounced group-specific 3D tumor genome conformations (**Figure 1c, Suppl.**  
125 **Figure 1c,d**). By an integrative analysis of the Hi-C data, enhancers (defined by H3K27ac ChIP-seq  
126 enrichments), and gene expression, we observed that genes are generally expressed at higher levels  
127 when their promoters physically interact with enhancers or other gene promoters (**Figure 1d**). A large  
128 percentage (~63-66%) of enhancer-associated genes (EAGs) previously predicted to be regulated by  
129 PFA or RELA enhancers<sup>18</sup> can be confirmed to have chromatin interactions between gene promoters  
130 and enhancers by the analysis of subgroup-specific Hi-C maps (**Figure 1e**). For example, the *Tenascin*  
131 *C* (*TNC*) promoter physically interacts with distal PFA enhancers (**Figure 1f**), which are positively  
132 correlated with *TNC* expression across a cohort of 24 tumors from six different intracranial  
133 ependymoma groups (**Figure 1g, Suppl. Figure 1e**). Overall, we found that more than twice as many

134 genes as previously reported<sup>18</sup> are potentially regulated by proximal and distal ependymoma enhancers  
135 (**Figure 1h, Suppl. Table 2,3**). For example, the gene encoding Eukaryotic Translation Elongation  
136 Factor 1 Alpha 2 (*EEF1A2*) interacts with subgroup specific enhancers (**Figure 1i**) and is specifically  
137 upregulated in *RELA* -fusion associated tumors (**Figure 1j**). These and other regulatory dependencies  
138 were not recognized in our previous study<sup>18</sup>, due to lack of data on chromatin interactions in  
139 ependymoma samples and because TAD annotations from a fetal lung fibroblast cell line (IMR90)  
140 were used instead (**Suppl. Figure 1f,g**).

141

#### 142 ***Transcriptional activation of RCOR2 by neo-TAD formation in supratentorial RELA ependymoma***

143 The formation of new topologically associating domains ('neo-TADs') through structural variation  
144 was recently shown to have a critical role in gene dysregulation and oncogenesis<sup>19,20</sup>. To dissect the  
145 effect of structural variants (SVs) in supratentorial *RELA* tumors on the potential formation of neo-  
146 TADs, we used newly developed computational tools for the detection of SVs based on Hi-C data<sup>19,21</sup>  
147 (**Suppl. Table 4**). We first took a closer look at the *C11orf95* and *RELA* gene loci, because it was  
148 previously shown that the oncogenic *C11orf95-RELA* gene fusions are a result of chromothriptic  
149 events on chromosome 11. As expected, the Hi-C data reproducibly detected structural variants at the  
150 *C11orf95* and *RELA* gene loci in the supratentorial *RELA* but not in PFA tumors (**Figure 2a, Suppl.**  
151 **Figure 2a**). Furthermore, the Hi-C data captured extraordinarily complex rearrangements within  
152 chromosome 11 in some *RELA* ependymoma samples (**Figure 2b**) and revealed that SVs are not  
153 restricted to chromosome 11 but also include inter-chromosomal rearrangements (**Figure 2c**). In  
154 particular, we observed intra- and inter-chromosomal structural variants in all *RELA* tumors, which  
155 lead to the formation of neo-TADs placing the *REST Corepressor 2 (RCOR2)* gene in a new regulatory  
156 environment (**Figure 2d, Suppl. Figure 2b**). *RCOR2* is located ~150kb away of *C11orf95* and has a  
157 strong enhancer element upstream of its transcription start site that forms new DNA interactions with  
158 the *C11orf95* gene and other nearby enhancer elements by bridging the *C11orf95-RELA* breakpoint  
159 (**Figure 2e, Suppl. Figure 2c**). By evaluating global Affymetrix gene expression array data<sup>1</sup> across  
160 ependymoma groups, we found that *RCOR2* expression is significantly upregulated in supratentorial  
161 *RELA* relative to other ependymoma groups (p-value=1.71e-91, **Figure 2f**) and is highly correlated  
162 with *C11orf95* transcription (R=0.66, p-value=6.93<sup>-11</sup>, **Suppl. Figure 2d**). Interestingly, we also  
163 identified *RCOR2* as a hit in *RELA* cells in an independent shRNA screen (data not shown). To  
164 validate the relevance of *RCOR2* for tumor growth and maintenance, we performed shRNA-mediated  
165 knock-down of *RCOR2* expression in patient derived *RELA* and PFA ependymoma cell lines. We  
166 observed that *RCOR2* knockdown results in strongly reduced cell survival of supratentorial *RELA* and  
167 to a lesser extent of PFA cell lines (**Figure 2g-h**). The on-target effect of shRNAs against *RCOR2* was



168 confirmed by western blot analysis of RCOR2 protein in RELA ependymoma cells (**Suppl. Figure**  
169 **2e**). RCOR2 can form a protein complex with the histone de-methylase LSD1, also known as KDM1A,  
170 and other transcriptional co-repressors, including HDAC1/2<sup>22</sup>. LSD1, HDAC1 and HDAC2 are all  
171 highly expressed across ependymoma subgroups and HDAC1/2 show pronounced RELA  
172 ependymoma-specific expression (**Suppl. Figures 2f-h**). Since there is no available compound against  
173 RCOR2, we reasoned that inhibition of other components of the RCOR2/LSD1/HDAC complex may  
174 still confer a therapeutic vulnerability for RELA ependymoma tumors. shRNA-mediated inhibition of  
175 *LSD1* expression indeed leads to a significant depletion of RELA but not PFA ependymoma cells  
176 compared to scrambled shRNA (**Figure 2i, Suppl. Figures 2i,j**). Surprisingly, however, targeting the  
177 enzymatic activity of LSD1 with the LSD1 inhibitor ORY-1001<sup>23</sup> had no effect on cell survival using  
178 clinically accessible concentrations (**Figure 2j**), suggesting that in this protein complex the protein  
179 rather than the enzymatic activity of LSD1 is important. In contrast, targeting the HDAC activity in  
180 the complex with Entinostat, an HDAC1-3 inhibitor, strongly inhibited the survival of RELA  
181 ependymoma cells, while having less effect on PFA cells (**Figure 2k**). Combining ORY-1001 with  
182 Entinostat showed no synergy (data not shown) and also the results for Corin, a dual inhibitor of both  
183 LSD1 and HDACs, were not better than those for Entinostat alone (**Figure 2l**). Inhibition of other  
184 HDACs with, e.g., HDAC8 and HDAC6/10 inhibitors PCI-34051 and Tubastatin, respectively, had no  
185 effect on cell survival (**Suppl. Figure 2k-l**). Altogether, our data show that the CoREST protein  
186 complex containing RCOR2, LSD1 and HDAC1/2 has a crucial role in the growth and maintenance  
187 of supratentorial RELA ependymoma tumors that can be inhibited by disrupting the complex or by  
188 targeting the activity of HDACs.

189

### 190 ***PFA Ependymomas are dependent on integrin $\alpha 6$***

191 In all PFA tumors the Hi-C data revealed a 3D chromatin cluster that spatially links numerous  
192 regulatory sequences and genes located more than 4 million base pairs apart on chromosome 2 (**Figure**  
193 **3a-c, Suppl. Figure 3a**). To determine if this chromatin cluster is specific to PFA tumors, we analyzed  
194 Hi-C data obtained from RELA ependymoma samples as well as normal human tissues and cell types  
195 analyzed by the ENCODE and PsychENCODE consortia<sup>24,25</sup>. There was no sign of similar DNA  
196 interactions in the RELA and non-tumor samples, suggesting that this chromatin cluster is specific to  
197 PFA ependymomas (**Figure 3a, Suppl. Figure 3a**). By analyzing the expression of genes in this  
198 chromatin cluster in ependymoma and normal human brain samples, we observed that *integrin  $\alpha 6$*   
199 (*ITGA6*) expression, encoding the receptor of the extracellular matrix protein laminin, is significantly  
200 upregulated in PFA compared to RELA ependymoma and also normal human brain tissues (p-value:

201 1.21e-114, **Suppl. Figure 3b**). As also reported previously<sup>1</sup>, gene-ontology analysis shows that  
202 ITGA6-associated gene sets, such as *extracellular matrix organization* and *positive regulation of cell*  
203 *migration*, are among the most highly enriched biological processes when comparing overall gene  
204 expression profiles of PFA to other ependymoma groups (**Suppl. Table 5**). Recent genome-wide  
205 CRISPR-Cas9 inhibition screens have revealed that ITGA6 is highly and specifically essential in PFA  
206 ependymoma cell lines compared to glioblastoma (GBM) cell lines and fetal neural stem cells  
207 (fNSCs)<sup>26,27</sup> (**Suppl. Figure 3c**). In addition, we find that *integrin  $\beta$ 4* (*ITGB4*), but not  *$\beta$ 1* (*ITGB1*), is  
208 significantly up-regulated in PFA compared to RELA ependymoma and normal brain samples (p-  
209 values: 1.48e-119 and 1.42e-90, **Suppl. Figure 3d**), suggesting that the integrin  $\alpha$ 6 $\beta$ 4 heterodimer is  
210 the functional form relevant for PFA tumors. Based on these results, we hypothesized that PFA  
211 ependymomas are locked in an oncogenic genomic topological configuration that activates *ITGA6*  
212 transcription and drives the acquisition and maintenance of stemness. To test this hypothesis, we  
213 performed CRISPR-Cas9 mediated *ITGA6* knock-out in patient-derived PFA ependymoma cells by  
214 cloning three different sgRNA sequences targeting *ITGA6* into a lentiviral vector expressing Cas9 in  
215 conjunction with GFP and subsequently transduced PFA ependymoma cells with the virus. As a result,  
216 we observe that transduced PFA ependymoma cells (**Figure 3d**), but neither transduced RELA  
217 ependymoma (**Suppl. Figure 3e**) nor glioblastoma cells (**Suppl. Figure 3f**), showed a gradual  
218 decrease in cell proliferation over time, validating *ITGA6* as an essential tumor-dependency gene  
219 specific for PFA ependymomas.

220

### 221 ***Transcriptional activation of LAMC1 as a potential resistance mechanism in recurrent PFA*** 222 ***tumors***

223 Conventional copy-number variation (CNV) analyses previously showed 1q copy-number gains in a  
224 subset of very aggressive and recurrent PFA ependymomas (**Suppl. Figure 3g**)<sup>10</sup>. By investigating  
225 CNVs in PFA tumors, including primary and relapse tumors of the same patient, we observed frequent  
226 increases in genomic instability in relapse tumors, while the 1q gain is maintained or emerges during  
227 tumor progression (**Suppl. Figure 3h**). To elucidate the molecular mechanisms associated with 1q  
228 gain, we systematically searched for SVs in all PFA ependymoma samples using the Hi-C data (**Suppl.**  
229 **Table 6**). As expected, primary PFA EPNs have frequent DNA interactions within chromosomes  
230 ('cis') and no DNA interactions indicative of recurrent structural variants (**Suppl. Figure 3i**).  
231 However, we observed several complex inter-chromosomal DNA ('trans') interactions indicative of  
232 structural variants in PFA ependymoma relapse tumors (**Figure 3e, Suppl. Figure 3j**). When  
233 comparing SVs among the analyzed PFA ependymoma relapse samples, we observed a recurring event  
234 that leads to an inversion of a ~66 Mb region of chromosome arm 1q into chromosome 8 (chr1-chr8

235 in sample EPD210FH, **Figure 3e**), or into chromosome 3 (chr1-chr3 in sample RD-19-157, **Suppl.**  
236 **Figure 3j**). In both cases, the breakpoints on chromosome 1q are located near the gene locus of *laminin*  
237 *subunit  $\gamma$ 1* (*LAMC1*). Examination of the Hi-C data shows that both SVs led to the formation of neo-  
238 TADs, which place *LAMC1* into new regulatory environments (**Figure 3f,g**). Inspecting RNA-seq  
239 expression data revealed that *LAMC1* is expressed almost three times higher in the two 1q+ PFA  
240 ependymoma relapse tumors than in primary PFA ependymoma tumors (**Figure 3h**). The same pattern  
241 of increased *LAMC1* expression in PFA relapse cases was found in a larger Affymetrix ependymoma  
242 data cohort<sup>1</sup> (**Figure 3i**). By a direct comparison of three relapse tumors that developed within 18 years  
243 after the primary diagnosis of a PFA ependymoma patient, we observed upregulation of *LAMC1*  
244 specifically in the third and fatal relapse tumor with marked chr1q gain (**Suppl. Figure 3h,k**). These  
245 results suggest that transcriptional activation of *LAMC1* by the formation of SV-induced neo-TADs is  
246 a resistance mechanism in recurrent 1q+ PFA EPN tumors that potentially promotes proliferation and  
247 stemness by further enhancing an already excessive integrin signaling. Based on these results, we  
248 hypothesized that *LAMC1* expression is essential for the proliferation and growth of PFA ependymoma  
249 tumors. To test this hypothesis, we performed genetic (CRISPR-Cas9) inhibition experiments against  
250 *LAMC1* and observed strongly reduced cell growth in the same PFA cell line EPD210FH that harbors  
251 the chr1-chr8 translocation (**Figure 3j, Suppl. Fig. 3l**) but not in RELA (**Suppl. Figure 3m**)  
252 ependymoma models.

### 253

### 254 *Hypermethylation disrupts CTCF binding in PFA ependymoma*

255 It has recently been shown that DNA methylation-mediated insulator dysfunction can lead to altered  
256 chromosomal topology thereby activating oncogenic programs (**Figure 4a**)<sup>28,29</sup>. Given the global loss  
257 of repressive H3K27me3<sup>10,11</sup> and a previously reported DNA methylation phenotype in PFA  
258 ependymoma<sup>5</sup>, we hypothesized that similar molecular mechanisms may drive oncogene activation in  
259 this tumor type. Therefore, we analyzed 7 PFA (n=4) and RELA (n=3) tumors using Whole Genome  
260 Bisulfite Sequencing (WGBS) and CTCF ChIP-seq (**Suppl. Table 1**). As expected, genome wide CpG  
261 methylation is high in PFA and RELA ependymomas with low levels of methylation at functional  
262 regulatory elements, such as promoters, enhancers and insulators (**Suppl. Figure 4a**). By comparative  
263 analysis of DNA methylation at CTCF binding sites, we found that DNA hypermethylation replaces  
264 2,387 CTCF binding sites in PFA tumors, but conversely is associated with the loss of only 178 CTCF  
265 binding sites in supratentorial RELA tumors (**Figure 4b-d**). The loss of CTCF binding through DNA  
266 hypermethylation is a predominant event in PFA ependymoma (**Figure 4c**) and can be associated with  
267 the formation of new enhancer-gene DNA loops and transcriptional activation of the target genes  
268 (**Suppl. Table 7**). To investigate whether such potential DNA methylation-mediated insulator

269 dysfunctions can be linked to the transcriptional activation of genes essential for PFA ependymoma,  
270 we compared our results with those of a genetic inhibition screen in PFA cell lines<sup>26</sup>. Among others,  
271 we observed localized hypermethylation in PFA tumors associated with the loss of a CTCF binding  
272 site and the formation of DNA interactions between non-coding regulatory enhancer elements and the  
273 *ADP Ribosylation Factor Like GTPase 4C (ARL4C)* gene (**Figure 4e-f**). *ARL4C* transcription is  
274 significantly (**p-value:** 4.25e-55) upregulated in PFA tumors compared to other ependymoma groups  
275 (**Suppl. Figure 4b**) and is highly correlated with the activity of the enhancer elements that physically  
276 interact with the *ARL4C* gene locus in PFA tumors (**Figure 4g, Suppl. Figure 4c**), but not in RELA  
277 tumors. It has been shown that *ARL4C* promotes migration, invasion and proliferation in colorectal  
278 and lung cancer<sup>30</sup> and recent genome-wide CRISPR-Cas9 inhibition screens revealed that *ARL4C* is  
279 essential for the proliferation of PFA ependymoma compared to glioblastoma cell lines (**Suppl. Figure**  
280 **4d**)<sup>26,27</sup>. By genetic (CRISPR-Cas9) inhibition experiments we validated that *ARL4C* is highly and  
281 specifically essential for the growth of PFA ependymoma (**Figure 4h**) compared to RELA  
282 ependymoma and glioblastoma models (**Suppl. Figure 4e-f**). These results not only provide additional  
283 evidence for the relevance of *ARL4C* in PFA ependymoma tumors, but also shed light on the various  
284 molecular mechanisms that potentially lead to oncogenic activation of gene expression through  
285 genome-wide epigenetic alterations.

286  
287

## 288 **Discussion**

289 By investigating 3D ependymoma genomes using Hi-C, we have identified multiple oncogenic  
290 chromatin conformations and novel tumor-dependency genes, pathways and potential therapeutic  
291 targets in RELA and PFA ependymoma. We show that structural variants in supratentorial tumors not  
292 only lead to *C11orf95-RELA* fusion genes, but also result in the formation of new regulatory  
293 environments that are recurrently associated with the aberrant overexpression of *RCOR2*. *RCOR2* is  
294 the scaffold protein in the CoREST complex that further contains LSD1 and HDAC1 and HDAC2.  
295 The complex is associated with gene silencing and is known to play a role in cancer development<sup>31</sup>.  
296 Here, we have shown that both *RCOR2* and *LSD1* expression is essential in RELA ependymoma, but  
297 not or to a lesser extent in PFA ependymoma, and that the cells are sensitive to HDAC1/2 inhibitors  
298 in line with our previous observations<sup>32</sup>. However, inhibition of the enzymatic activity of LSD1 had  
299 no effect. These results suggest that the activities of HDAC1/2 may be critical in regulating CoREST  
300 repressor functions in RELA ependymoma. Recent work in small cell lung cancer (and Merkel cell  
301 carcinoma) also implicated that disrupting the CoREST complex, but not the inhibition of LSD1's  
302 enzymatic activities is required for blocking cancer cell proliferation<sup>33</sup>. Further studies identifying the

303 components of the CoREST complex and identifying drugs that can disrupt the complex will be  
304 instrumental in developing an effective CoREST-targeted therapy for RELA ependymoma.  
305 Furthermore, we have shown that PFA ependymomas are not only characterized by diminished histone  
306 methylation and increased acetylation at histone 3 lysine 27 (H3K27), as recently reported<sup>26</sup>, but also  
307 exhibit a tumor-specific 3D chromatin organization. Through targeting of *ITGA6*, a gene involved in  
308 a PFA-specific chromatin cluster, we demonstrate the importance of integrin signaling for maintained  
309 tumor growth, specifically in PFA tumors. *ITGA6* has been described as a marker for cancer stem cells  
310 (CSCs) in several cancer types<sup>34-38</sup>, where disruption of *ITGA6* function suppresses the CSC phenotype  
311 and the maintenance of stem cells<sup>34</sup>. Our results provide evidence for an epigenetic dysregulation event  
312 that promotes integrin signaling and the acquisition of stemness in PFA ependymoma. The significance  
313 of integrin signaling for PFA tumor progression is further promoted by the recurrent transcriptional  
314 activation of *LAMC1* in PFA relapse tumors which frequently harbor gains of chromosome 1q.  
315 Although relapse tumors often show increased genomic instability, our Hi-C data showed for the first  
316 time an unexpected complexity of intra- and inter- chromosomal rearrangements underlying some  
317 chromosome-arm-wide copy number variations. Our results suggest that transcriptional activation of  
318 *LAMC1* by the formation of SV-induced neo-TADs is a potential resistance mechanism in recurrent  
319 1q+ PFA EPN tumors that promotes proliferation and stemness by further enhancing already excessive  
320 integrin signaling. For other tumor types, *LAMC1* has already been shown to be involved in tumor  
321 cell invasion and metastasis<sup>39</sup>. Thus, strategies that target integrin signaling, including *ITGA6* and  
322 *LAMC1*, may reveal new vulnerabilities and overcome resistance to therapy in the treatment of PFA  
323 EPN relapse patients. Insulator dysfunction and oncogene activation by hypermethylation of CTCF  
324 binding sites has recently been described in IDH mutant gliomas and in SDH-deficient gastrointestinal  
325 stromal tumors (GISTs)<sup>28,29</sup>. Here, we show that PFA ependymoma is another tumor type with a global  
326 epigenetic phenotype in which there is hypermethylation of CTCF binding sites and associated  
327 changes in genome topology. By genetic inhibition of *ARL4C* in a PFA ependymoma model, we  
328 provide evidence that insulator dysfunction is a potential oncogenic mechanism in PFA ependymoma  
329 tumors and that tumor-dependency genes can be identified by 3D tumor genome profiling. Altogether,  
330 our study has identified several new group specific tumor dependencies in ependymoma, opening up  
331 avenues for potential novel therapeutic interventions that are highly needed in this disease, especially  
332 for RELA and PFA ependymoma. Our results will also be important for other (pediatric) cancers,  
333 especially those that relapse, where the drivers might be known, but where therapeutic options are  
334 scarce. Hi-C studies in these tumors may also reveal unknown tumor dependencies and new  
335 therapeutic targets.

336

337 **Figures**

338

339 **Figure 1: 3D tumor genome profiling identifies PFA and RELA specific chromatin**

340 **conformations and ependymoma enhancer associated genes.**

341 **(a)** Overview of the major results obtained by the application of genome-wide chromosome  
342 conformation capture (Hi-C) in ependymoma brain tumors.

343 **(b)** Characteristics of ependymoma samples analyzed by Hi-C. One group of PFA ependymoma  
344 samples has no apparent copy-number variants, while the other group of PFA samples exhibits  
345 chromosome 1q gains associated with an unfavorable outcome.

346 **(c)** Unsupervised hierarchical clustering of PFA and RELA ependymoma tumors based on DNA  
347 interactions (Hi-C) stratifies the samples into the expected molecular groups.

348 **(d)** Integrative analysis of enhancers (H3K27ac ChIP-seq), chromosome conformation (Hi-C) and  
349 gene expression (RNA-seq) shows that genes are more strongly expressed when their promoters  
350 physically interact with other promoters or with enhancers. Shown are tumors (3x PF-A, 3x RELA)  
351 for which sample-matched H3K27ac ChIP-seq, RNA-seq, and HiC data are available. The center  
352 line, box limits and whiskers indicate the median, upper/lower quartiles and 1.5× interquartile range  
353 respectively. P-values from the bootstrap t-test are included.

354 **(e)** Re-evaluation of genes previously predicted to be regulated by PFA ependymoma enhancers  
355 confirms that the promoter regions of approximately 66% of these genes (n=1,028) physically  
356 interact with PFA ependymoma enhancers. Similar results (63%, n=1,229) are obtained for RELA  
357 ependymomas.

358 **(f)** The *TNC* promoter physically interacts with two distal enhancers (E1 and E2), whereby the  
359 interaction with the more proximal enhancer E1 is much more pronounced in PFA than in RELA  
360 tumors.

361 **(g)** *TNC* expression is positively correlated with the activity of the PFA-specific enhancer E1  
362 (*chr9:118146925–118163777*), which is located 390kb upstream of the *TNC* transcription start site.  
363 Here, a cohort of 24 tumors from six different intracranial ependymoma groups was examined.

364 **(h)** The integrative analysis of Hi-C, enhancer and gene expression data reveals that more than twice  
365 as many genes as previously reported<sup>18</sup> are regulated by proximal and distal ependymoma enhancers.

366 **(i)** The Hi-C data identifies a cluster of DNA interactions between a RELA-specific superenhancer  
367 (SE) and the *EEF1A2* gene. This regulatory dependency was not recognized previously because Hi-  
368 C data obtained from IMR90 cells, which is commonly used as a reference, does not show any DNA  
369 interactions and topologically associated domains at the *EEF1A2* gene locus.

370 **(j)** *EEF1A2* expression is positively correlated with the RELA-specific SE  
371 (*chr20:62060923–62127745*) highlighted in panel i. This regulatory dependency is further supported  
372 by the many RELA-specific DNA interactions observed in the Hi-C data.

373

374 **Figure 2: Transcriptional activation of *RCOR2* by neo-TADs in RELA ependymoma**

375 **(a)** The Hi-C data reliably detect the structural variants that lead to the *C11orf95-RELA* fusion gene  
376 in supratentorial RELA-fusion associated tumors. Green boxes highlight SVs predicted by the  
377 computational methods applied.

378 **(b)** Chromothriptic rearrangements of chromosome 11 in a patient-derived RELA cell line (RELA  
379 BT165) visualized using Hi-C data.

380 **(c)** Structural variants in RELA tumors are not limited to chromosome 11 but also involve other  
381 chromosomes. Shown is an inter-chromosomal structural variant that includes chr11 and chr22 in  
382 tumor sample 7EP41.

383 **(d)** Reconstruction of the *C11orf95-RELA* breakpoint in a supratentorial tumor (4EP35) using Hi-C  
384 data reveals the formation of a neo-TAD that involves DNA interactions between *RCOR2* and the  
385 *C11orf95-RELA* fusion gene. RNA-seq and H3K27ac ChIP-seq data of this sample are included as  
386 additional tracks.

387 **(e)** Genome browser visualization of the *C11orf95* and *RCOR2* genomic region shows RELA  
388 ependymoma-specific enhancers and DNA interactions.

389 **(f)** Boxplot of *RCOR2* gene expression across ependymoma groups using Affymetrix gene  
390 expression data (n=393). The center line, box limits, whiskers and points indicate the median,  
391 upper/lower quartiles, 1.5× interquartile range and outliers, respectively. *RCOR2* is significantly  
392 upregulated in RELA tumors (anova p-val.: 1.71e-91).

393 **(g-i)** shRNA time-course knockdown experiments in RELA (EP1NS) and PFA (EPD210FH)  
394 ependymoma cell lines using a scrambled control and two shRNA constructs each targeting either  
395 *RCOR2* in EP1NS **(g)**, *RCOR2* in EPD210FH **(h)** or *LSD1* in EP1NS **(i)**. All constructs are GFP  
396 tagged and GFP positive cells are sorted by FACS. Results are normalized to day 0 and error bars  
397 represent SEM from two independent experiments.

398 **(j-l)** Dose response curves of single-compound treatment with ORY-1001 **(j)**, Entinostat **(k)** or Corin  
399 **(l)** of RELA (EP1-NS) and PFA (EPD210FH) ependymoma spheroids over a 72-hour time-course  
400 using Celltiter-Glo cell viability assays. For each sample the results are presented as percentage of  
401 the Luminescence signal from control condition (i.e. water for ORY-1001 and DMSO for Entinostat  
402 and Corin as a vehicle). Data are presented as SEM from three independent experiments per tumor  
403 type.

404

405 **Figure 3: PFA Ependymomas are dependent on integrin signaling**

406 **(a)** Hi-C DNA interaction matrices wherein a ~5 million base pair segment of chromosome 2 is  
407 aligned along the diagonals shown for PFA (9EP1, left) and RELA (4EP53, middle) tumors and  
408 normal cerebellum astrocytes (CAs, right). Off-diagonal signals indicate DNA interactions between  
409 different genomic sites. The chromatin complex (highlighted by dashed circles) spatially links  
410 several genes, including *ITGA6*, and various regulatory elements located more than 4 million base  
411 pairs apart and is recurrently observed in all PFA ependymoma tumors, but in none of the other  
412 samples analyzed.

413 **(b)** Hi-C DNA interactions of a PFA tumor (sample BT214) wherein the same ~5 million base pair  
414 segment of chromosome 2 shown in panel (a) is aligned horizontally. Circles and dashed lines  
415 highlight long-range DNA interactions.

416 **(c)** Genome browser view of the PFA-specific chromatin cluster shown in panels (a) and (b). The  
417 included data tracks show long-range DNA interactions in PFA tumors ('Hi-C loops') as well as  
418 gene expression and H3K27ac in RELA and PFA tumors.

419 **(d)** Genetic (CRISPR-Cass9) time-course knockout of *ITGA6* in PFA ependymoma cells  
420 (EPD210FH) using an unspecific control and three individual sgRNA constructs. All constructs are  
421 GFP tagged and GFP positive cells are sorted by FACS. Results are normalized to day 0 and error  
422 bars represent SEM from two independent experiments.

423 **(e)** The conventional copy number profile of a PFA relapse sample (EPD210FH) shows high  
424 genomic instability including gain of chromosome arm 1q (presented vertically on the left). The  
425 genome-wide DNA interaction (Hi-C) map obtained from the same sample identifies complex inter-  
426 chromosomal structural variants including an inversion that involves chr1q and chr8. These trans-  
427 SVs reveal the complexity of genomic rearrangements underlying some copy-number gains and  
428 losses observed by common copy number variation analyses.

429 **(f)** Re-construction of the structural variant that involves chr1q and chr8 in the PFA relapse sample  
430 EPD210FH using Hi-C data. This structural variant results in the formation of a neo-TAD that places  
431 the *LAMCI* gene locus in a new regulatory environment.

432 **(g)** Re-construction of the structural variant that involves chr1q and chr3 in the PFA relapse tumor  
433 RD-19-157 using Hi-C data obtained from FFPE material. This structural variant also results in the  
434 formation of a neo-TAD that places the *LAMCI* gene locus in a new regulatory environment.

435 **(h)** Boxplot of RNA-seq expression analysis revealed that *LAMCI* is expressed almost three times  
436 higher in the two 1q+ PFA ependymoma relapse tumors than in primary PFA tumors, suggesting that  
437 the transcriptional activation of *LAMCI* by the formation of SV-induced neo-TADs is a common



438 resistance mechanism in recurrent 1q+ PFA EPN tumors. The center line, box limits, whiskers and  
439 circles indicate the median, upper/lower quartiles, 1.5× interquartile range and samples, respectively.  
440 **(i)** Boxplot of Affymetrix gene expression data shows that *LAMC1* tends to be upregulated in a  
441 larger cohort of relapse PFA in comparison to primary PFA ependymoma tumors. The center line,  
442 box limits, whiskers and points indicate the median, upper/lower quartiles, 1.5× interquartile range  
443 and outliers, respectively.  
444 **(j)** Genetic (CRISPR-Cas9) time-course knockout of *LAMC1* in PFA ependymoma cells  
445 (EPD210FH) using an unspecific control and three individual sgRNA constructs. All constructs are  
446 GFP tagged and GFP positive cells are sorted by FACS. Results are normalized to day 0 and error  
447 bars represent SEM from two independent experiments.

448

449 **Figure 4. Hypermethylation replaces CTCF binding sites in PFA ependymoma.**

450 **(a)** Proposed mechanism of epigenetic oncogene activation in PFA ependymoma tumors. Top: The  
451 oncogene is separated from an enhancer by a CTCF insulator, which forms a topological barrier.  
452 Below: The CTCF insulator is replaced by DNA methylation so that the enhancer can contact the  
453 oncogene and enhances its expression.  
454 **(b)** The volcano plot shows significant differential CTCF binding sites between PFA and RELA  
455 ependymoma tumors (min *p-value*: 0.1). CTCF binding sites significantly hypermethylated in PFA  
456 relative to RELA tumors are marked in orange (min *q-value*: 0.05).  
457 **(c)** Comparison of CTCF binding strength (CTCF ChIP-seq, x-axis, min *p-value* 0.1, min fold  
458 change: 0.5) and DNA methylation (WGBS, y-axis, min *q-value*: 0.05, min difference: 0.1) at CTCF  
459 binding sites that show significant differences between PFA and RELA ependymoma tumors.  
460 **(d)** Heatmap of WGBS-derived DNA methylation at the 300 most significant CTCF binding sites  
461 lost in three PFA (left) and three RELA (right) ependymoma tumors. The heatmaps and the  
462 composite panels on top show that CTCF binding sites are commonly replaced by DNA methylation  
463 in PFA tumors.  
464 **(e)** Genome browser visualization of PFA ependymoma-specific DNA loops that associate two PFA  
465 enhancers (E1 and E2) with the *ARL4C* gene locus located ~3,520 kbp away from the *ARL4C*  
466 transcription start site.  
467 **(f)** WGBS-derived DNA methylation and CTCF ChIP-seq data from PFA and RELA ependymoma  
468 tumors show that a CTCF binding site separating the *ARL4C* gene from the E1 and E2 PFA  
469 enhancers is replaced by DNA methylation in PFA tumors.

470 **(g)** *ARL4C* gene expression is positively correlated with the activity of enhancer E2  
471 (*chr2:237763494–237764993*) across a cohort of 24 ependymoma tumors from six different  
472 intracranial ependymoma groups.

473 **(h)** Genetic (CRISPR-Cas9) time-course knockout of *ARL4C* in PFA ependymoma cells  
474 (EPD210FH) using an unspecific control and three individual sgRNA constructs. All constructs are  
475 GFP tagged and GFP positive cells are sorted by FACS. Results are normalized to day 0 and error  
476 bars represent SEM from two independent experiments.

477

478

### 479 **Supplementary Figure 1**

480 **(a)** The number of DNA contacts obtained in the individual ependymoma samples as a quality  
481 measure for the Hi-C data.

482 **(b)** The tSNE dimensionality reduction visualization and unsupervised clustering of DNA  
483 methylation data from a cohort of ependymoma samples (n=1,182) separates PFA and RELA  
484 ependymomas into separate groups. The samples analyzed in this study by Hi-C are highlighted in  
485 red and orange. Blocks marked with an asterisk show a magnification of selected samples, for better  
486 visualization.

487 **(c)** Proportions of topologically associated domains (TADs) shared between ependymoma tumors.  
488 The comparison is performed among PFA (n=3) and RELA (n=3) ependymoma tumors that were  
489 also included in our previous enhancer-mapping study<sup>18</sup>. Hi-C data from two normal cerebellum  
490 astrocytes provided in the ENCODE database<sup>40</sup> were included as controls. The mean proportion of  
491 common TADs is 0.569 and the greatest similarity is found in TADs from samples of the same group  
492 (PFA, RELA and cerebellar astrocytes), while the common TAD proportions in the individual  
493 sample groups are smaller.

494 **(d)** Numbers of common TADs between EPN PFA (n=3) and RELA (n=3) samples from enhancer  
495 landscape study. The highest number of same TADs is among all samples.

496 **(e)** *TNC* expression is positively correlated across a cohort of 24 tumors from six different  
497 intracranial ependymoma groups with the activity of the PFA ependymoma-specific enhancer E2  
498 (*chr9:118275447–118288653*) located upstream of the *TNC* transcription start site.

499 **(f-g)** Hi-C data visualization of a genomic region that includes the *EEF1A2* gene. The association  
500 between a RELA ependymoma super enhancer (SE) and the up regulation of *EEF1A2* transcription  
501 was not detected previously due to the lack of annotated TADs at this gene locus in the Hi-C data  
502 from IMR90 samples. TADs derived from IMR90 (blue), RELA (RELA BT, red), and PFA  
503 (EPD210FH, orange) ependymoma samples are visualized in boxes.

504

505 **Supplementary Figure 2**

506 **(a)** Visualization of the Hi-C data at the extended *C11orf95* and *RELA* gene locus in PFA  
507 ependymoma tumors shows the absence of structural variants.

508 **(b)** Reconstruction of the *C11orf95-RELA* breakpoint in *RELA* ependymoma tumors (7EP41 and  
509 11EP22) using Hi-C data reveals the formation of a neo-TAD that involves DNA interactions  
510 between *RCOR2* and the *C11orf95-RELA* fusion gene. RNA-seq, CTCF and H3K27ac ChIP-seq data  
511 of these samples are included as additional tracks.

512 **(c)** Chr11 genome browser visualization showing DNA loops that span the *C11orf95* and *RELA* gene  
513 loci.

514 **(d)** Correlation between the expression of *RELA* and *RCOR2* ( $R=0.663$ ,  $p\text{-val}=6.93\text{e-}11$ ) in *RELA*  
515 ependymoma tumors ( $n=76$ ) profiled by Affymetrix gene expression arrays.

516 **(e)** Knock-down of *RCOR2* expression in *RELA* ependymoma cells. Western blots show protein  
517 levels 4 days post infection with indicated shRNAs. B-actin is used as a loading control.

518 **(f-h)** Boxplots of *LSD1*, *HDAC1* and *HDAC2* gene expression across ependymoma subgroups using  
519 Affymetrix gene expression data ( $n=393$ , anova p-values:  $9.77\text{e-}15$ ,  $1.02\text{e-}27$ ,  $1.20\text{e-}14$ ). The center  
520 line, box limits, whiskers and points indicate the median, upper/lower quartiles,  $1.5\times$  interquartile  
521 range and outliers, respectively.

522 **(i)** Knock-down of *LSD1* expression in ependymoma cells. Western blots show protein levels 4 days  
523 post infection with indicated shRNAs. B-actin is used as a loading control.

524 **(j)** shRNA time-course knockdown experiments in a PFA ependymoma cell line (EPD210FH) using  
525 a scrambled control and two shRNA constructs targeting *LSD1*. All constructs are GFP tagged and  
526 GFP positive cells are sorted by FACS. Results are normalized to day 0 and error bars represent  
527 SEM from two independent experiments.

528 **(k-l)** Dose response curves of the HDAC8 inhibitor PCI-34051 **(k)** and the HDAC 6/10 inhibitor  
529 Tubastatin **(l)** treatment of *RELA* (EP1NS, red) and PFA (EPD210FH, orange) ependymoma  
530 spheroids over a 72-hour time-course using Celltiter-Glo cell viability assays. For each sample, the  
531 results are presented as percentage of the Luminescence signal from control condition (DMSO as a  
532 vehicle). Data are presented as SEM from three independent experiments per tumor type.

533

534 **Supplementary Figure 3**

535 **(a)** DNA interaction matrices derived from HiC data wherein a  $\sim 5$  million base pair segment of  
536 chromosome 2 (172,407,031-177,907,030 bp) is aligned along the diagonals. Off-diagonal signals  
537 indicate DNA interactions between different genomic sites. The chromatin complex at the *ITGA6*

538 locus recurrently forms in all PFA EPN tumors analyzed (shown for samples 9EP1, 9EP9, and  
539 7EP18 in the top row). This chromatin complex is not present in RELA endependymoma tumors  
540 (middle row). Moreover, normal human cell types analyzed by the ENCODE and PsychENCODE  
541 consortia, such as cerebellar astrocytes (CA), neural progenitor cells (NPCs) and embryonic  
542 fibroblasts (IMR90, bottom row), do not show signs of similar DNA interactions, suggesting that this  
543 chromatin complex is characteristic for PFA endependymoma tumors.

544 **(b)** Differential gene expression analysis of Affymetrix array data identified *ITGA6* as significantly  
545 (FDR<0.01, two-sided Wilcoxon test) upregulated in PFA compared to RELA endependymoma tumors  
546 and normal brain samples (n=200 PFA, n=76 RELA, and n=225 normal human brain samples). In  
547 the boxplot the center line, box limits, whiskers and points indicate the median, upper/lower  
548 quartiles, 1.5× interquartile range and outliers, respectively.

549 **(c)** *ITGA6* has been observed as an essential gene specifically in PFA endependymoma cell lines  
550 compared to glioblastoma stem cells (GSCs) and fetal neural stem cells (fNSCs) in a published  
551 CRISPR-Cas9 knock-out screen<sup>26</sup>. In the boxplot the center line, box limits and whiskers indicate the  
552 median, upper/lower quartiles and 1.5× interquartile range, respectively.

553 **(d)** Expression of two alternative *ITGA6* heterodimer partner proteins *ITGB1* and *ITGB4*. While  
554 *ITGB1* and *ITGB4* are highly expressed in PFA and RELA endependymoma tumors compared to normal  
555 brain samples, only *ITGB4* is significantly upregulated (FDR<0.01, two-sided Wilcoxon test) in PFA  
556 compared to RELA endependymoma tumors, suggesting that the integrin  $\alpha6\beta4$  heterodimer is the  
557 functional form relevant for PFA endependymoma tumors (n=200 PFA, n=76 RELA, and n=225 normal  
558 human brain samples). In the boxplots the center line, box limits, whiskers and points indicate the  
559 median, upper/lower quartiles, 1.5× interquartile range and outliers, respectively.

560 **(e)** Genetic (CRISPR-Cas9) time-course knockout of *ITGA6* in RELA endependymoma cells (EP1-NS)  
561 using an unspecific control and three individual sgRNA constructs. All constructs are GFP tagged  
562 and GFP positive cells are sorted by FACS. Results are normalized to day 0 and error bars represent  
563 SEM from two independent experiments.

564 **(f)** Genetic (CRISPR-Cas9) time-course knockout of *ITGA6* in glioblastoma (GBM2) cells using an  
565 unspecific control and three individual sgRNA constructs. All constructs are GFP tagged and GFP  
566 positive cells are sorted by FACS. Results are normalized to day 0 and error bars represent SEM  
567 from two independent experiments.

568 **(g)** Example of a copy number profile of a PFA endependymoma tumor (16EP7) harboring a 1q gain.  
569 The CNV profile was obtained from DNA methylation array data.

570 **(h)** Copy number profiles of a primary and three relapse PFA endependymoma tumors from the same  
571 patient (RD-19-157). The CNV profiles were obtained from DNA methylation array data.

572 **(i)** Visualization of Hi-C data obtained from a primary PFA ependymoma tumor (16EP7) harboring a  
573 1q gain shows frequent DNA interactions within chromosomes but no DNA interactions indicative  
574 of inter-chromosomal structural variants.

575 **(j)** The conventional copy number profile of a PFA relapse sample (RD-19-157) shows high  
576 genomic instability including gain of chromosome arm 1q (presented vertically on the left). The  
577 genome-wide DNA interaction (Hi-C) map obtained from the same sample identifies complex inter-  
578 chromosomal structural variants including an inversion that involves chr1q and chr3.

579 **(k)** Expression of *LAMC1* in the three relapse tumors of patient RD-19-157 shows up-regulation of  
580 *LAMC1* in the third relapse tumor that harbors a 1q gain.

581 **(l)** Western blots show efficacy of sgRNAs targeting *LAMC1* and control sgRNA in EPD210FH  
582 cells. Mixture of different clones of infected EPD210FH cells are used to obtain protein extracts at  
583 day 5 post infection with indicated sgRNAs. B-actin is used as a loading control.

584 **(m)** Genetic (CRISPR-Cas9) time-course knockout of *LAMC1* in RELA ependymoma (EP1-NS)  
585 cells using an unspecific control and three individual sgRNA constructs. All constructs are GFP  
586 tagged and GFP positive cells are sorted by FACS. Results are normalized to day 0 and error bars  
587 represent SEM from two independent experiments.

588

#### 589 **Supplementary Figure 4**

590 **(a)** Mean methylation of PFA and RELA ependymoma tumors at promoters, enhancers and CTCF  
591 binding sites. The center line, box limits, whiskers and points indicate the median, upper/lower  
592 quartiles, 1.5× interquartile range and outliers, respectively.

593 **(b)** Boxplot showing *ARL4C* gene expression across ependymoma subgroups (Affymetrix gene  
594 expression data for n=393 ependymoma tumors). The center line, box limits, whiskers and points  
595 indicate the median, upper/lower quartiles, 1.5× interquartile range and outliers, respectively. *ARL4C*  
596 is significantly upregulated in PFA compared to the other ependymoma types (anova p-val.: 4.25e-  
597 55).

598 **(c)** Positive correlation of *ARL4C* gene expression and the activity of enhancer E1  
599 (*chr2:237545700–237546199*) across a cohort of 24 ependymoma tumors from six different  
600 intracranial ependymoma groups.

601 **(d)** *ARL4C* has been observed as an essential gene in PFA ependymoma cell lines in a published  
602 CRISPR-Cas9 knock-out screen<sup>26</sup>. In the boxplot the center line, box limits and whiskers indicate  
603 the median, upper/lower quartiles and 1.5× interquartile range, respectively.

604 **(e)** Genetic (CRISPR-Cas9) time-course knockout of *ARL4C* in RELA ependymoma (EP1-NS) cells  
605 using an unspecific control and three individual sgRNA constructs. All constructs are GFP tagged

606 and GFP positive cells are sorted by FACS. Results are normalized to day 0 and error bars represent  
607 SEM from two independent experiments.

608 **(f)** Genetic (CRISPR-Cas9) time-course knockout of *ARL4C* in glioblastoma (GBM2) cells using an  
609 unspecific control and three individual sgRNA constructs. All constructs are GFP tagged and GFP  
610 positive cells are sorted by FACS. Results are normalized to day 0 and error bars represent SEM  
611 from two independent experiments.

612

## 613 **Supplementary Tables**

614

615 **Supplementary Table 1:** Cohort of ependymoma tumor samples and available data types.

616

617 **Supplementary Table 2:** Enhancer associated genes supported by DNA loops in PFA ependymoma.

618

619 **Supplementary Table 3:** Enhancer associated genes supported by DNA loops in RELA  
620 ependymoma.

621

622 **Supplementary Table 4:** Structural variants in RELA ependymoma samples as identified by  
623 (a) hicBreakFinder. No additional filter was applied. (b) HiC SV/trans with adjusted filtering.

624

625 **Supplementary Table 5:** DAVID Gene Ontology analysis results for differentially expressed genes  
626 specific for PFA compared to other ependymoma subgroups.

627

628 **Supplementary Table 6:** Structural variants in PFA ependymoma samples as identified by  
629 (a) hicBreakFinder. No additional filter was applied. (b) HiC SV/trans with adjusted filtering.

630

631 **Supplementary Table 7:** Enhancer-associated genes supported by DNA loops that are potentially  
632 formed due to the replacement of CTCF binding sites by DNA methylation in PFA ependymoma  
633 tumors.

634

635 **Supplementary Table 8:** Overview of shRNA and sgRNA oligo sequences applied in experimental  
636 validation.

637

638 **Supplementary Table 9:** Drugs selected for experimental validation

639

640 **Supplementary Table 10:** Overview of antibodies applied in experimental validation.

641

642

### 643 **Acknowledgements**

644 We are thankful to David T. Jones for providing pediatric patient-derived SU-pcGBM2 cells. This  
645 work is supported by a Hannah’s Heroes St. Baldrick’s Scholar Award (LC) and funding from the  
646 NIH National Institute of Neurological Disorders and Stroke Institute R21 NS116455 (LC), the NIH  
647 National Cancer Institute U01 CA217885 (JPM), U01 CA184898 (JPM), U24 CA210004 (JPM and  
648 JTR); the NIH National Institute of General Medical Sciences R01GM074024 (JPM); and the NIH  
649 National Library of Medicine T15LM011271 for OC. The pediatric brain profiling at NYU in M.S.  
650 laboratory was in part supported by grants from the Friedberg Charitable Foundation and the Making  
651 Headway Foundation. Work in the laboratory of J.R.D. was supported by a NIH Early Independence  
652 Award (DP5 OD023071).

653

654

### 655 **Contributions**

656 K.O., A.C., M.K. and L.C. prepared the manuscript and figures. K.O., O.C., A.C., M.P. J.T.R., E.F.J.  
657 and A.S. performed data analysis and visualization. A.C., D.E.P., M.M., and J.M.H. performed  
658 experimental validations, N.G.C., M.L., D.M., S.N., and M.S. processed and analyzed tumor  
659 material, R.B., S.C., K.K., R.A.H. and D.R. generated Hi-C libraries from frozen and FFPE tumor  
660 material and cell lines, K.W.P., T.M., S.M., A.S., H.C., J.C., R.W.R., K.A.M., S.A.K., M.D.T., F.B.,  
661 J.R., J.P.M., S.M.P., F.A. and J.R.D. contributed to the study design and data interpretation. L.C.  
662 designed the study and L.C. and M.K. co-supervised the project.

663

664

665

666

## 667 **Methods**

668

### 669 **Chromosome conformation capture**

670 Hi-C on frozen tumor tissue sample was carried out using protocols previously described for tissue Hi-  
671 C experiments<sup>41</sup>. In brief, frozen tissues are pulverized using a mortar and pestle kept cold on a bed of  
672 dry ice into a fine powder. The tissue powder was then transferred to a 15mL conical tube containing  
673 5mLs of DPBS and fixed with 2% formaldehyde for 10 minutes. The fixation was quenched by  
674 addition of 0.2M Glycine. The fixed tissue was pelleted by centrifugation, washed 1x with DPBS, and  
675 then flash frozen until ready for further processing.

676 For Hi-C experiments, the fixed frozen tissue pellets were first resuspended in 3mLs of lysis buffer  
677 (10mM Tris-HCl pH 8.0, 5mM CaCl<sub>2</sub>, 3mM MgAc, 2mM EDTA, 0.2mM EGTA, 1mM DTT, 0.1mM  
678 PMSF, 1X Complete Protease Inhibitors). The sample was transferred to an M-tube and dissociated  
679 using a GentleMACS Tissue dissociator (Miltenyi) using the “Protein M-tube” setting. The sample  
680 was removed from the M-tube into a 50mL conical. The M-tube was washed with 3mLs of lysis buffer  
681 with 0.4% Triton X-100 added, and this wash was combined with the original 3mLs of sample for a  
682 total volume of 6mLs with final concentration of 0.2% Triton X-100. The sample was then passed  
683 through a 40µM cell strainer. The strainer was washed with an additional 2mLs of lysis buffer with  
684 0.2% Triton X-100. The sample was then centrifuged and washed with 1mL of lysis buffer with 0.2%  
685 Triton X-100. After centrifugation, the sample was resuspended in 0.5% SDS and processed with  
686 previously described *in situ* Hi-C method<sup>42</sup> using the MboI enzyme. Libraries were prepared using the  
687 Illumina TruSeq LT sequencing adaptors. Initial QC sequencing was first performed on a MiSeq to  
688 assess library quality, and if sufficient, was subject to production scale sequencing on the HiSeq X or  
689 NovaSeq platform, respectively.

690

### 691 **Chromosome conformation capture from FFPE material**

692 Hi-C experiments on FFPE material were carried out by Arima Genomics, Inc (San Diego, CA).  
693 Dewaxed and re-hydrated FFPE tissue was used as input to a modified version of the Arima-HiC Kit  
694 protocol. After the Arima-HiC protocol, Illumina-compatible sequencing libraries were prepared by  
695 shearing the proximally ligated DNA and then size-selecting DNA fragments using SPRI beads. The  
696 size-selected fragments containing ligation junctions were enriched using Enrichment Beads (provided  
697 in the Arima-HiC Kit), and converted into Illumina-compatible sequencing libraries using the Swift  
698 Accel-NGS 2S Plus kit (P/N: 21024) reagents. After adapter ligation, DNA was PCR amplified and



699 purified using SPRI beads. The purified DNA underwent standard QC (qPCR and Bioanalyzer) and  
700 sequenced on the NovaSeq following manufacturer's protocols.

701

### 702 **Hi-C data processing**

703 The sequencing reads alignment to hg19 human genome reference and chromatin contacts calling was  
704 performed using HiCPro 2.9.0 toolkit<sup>43</sup> allowing the bin sizes 5,10,50,100,250 and 500 Kbp. Main  
705 visualization and normalized full contacts extraction was performed with JuiceBox v0.7.5 toolkit<sup>44</sup> .  
706 Per sample loop calling was applied from FitHiC v2.0.6 method<sup>45</sup> on bin sizes 5 Kbp with maximum  
707 distance between bins 50 Mbp. TAD calling was performed based on 50 Kbp bins resolution using  
708 TopDom tool<sup>46</sup>.

709

### 710 **Unsupervised clustering of Hi-C data**

711 Hi-C data processing produced interaction matrices in .juicebox format for 3 RELA and 8 PFA  
712 ependymoma tumors. For each tumor, unsupervised clustering features were computed using the  
713 *Eigenvector* utility from the Juicer Tools analysis toolkit.<sup>47</sup> Briefly, the Eigenvector utility computes  
714 A/B compartments as the first principal component of the Pearson correlation matrix of each intra-  
715 chromosomal contact matrix.<sup>48</sup> A/B compartments were computed using Knight-Ruiz normalization  
716 at 1Mb resolution. Unsupervised hierarchical clustering was performed on these features using Pearson  
717 correlation distance and average linkage, using the *heatmap.2* function from *gplots* R package.

718

### 719 **Genes and enhancers connections via loops**

720 The ChIP-seq derived enhancer signals along with genomic locations of group-specific enhancers and  
721 normalized RNA-seq gene expression profiles from ependymoma tumors cohort (n=25) were obtained  
722 from published materials of the corresponding study<sup>18</sup>. Genome was fragmented into 5 Kbp bins and  
723 output from FitHiC loop calling tool was used to find contacts between genes and enhancers. For this  
724 purpose the genes were assigned to bins based on the location of transcription start site (TSS, 2500  
725 Kbp upstream and downstream of the gene start loci), while enhancers based on the overlap. Loop  
726 boundary correspondence was assigned to gene and/or group-specific enhancer lying either within the  
727 bin or in the closest upstream/downstream bin. Enhancer associated gene was considered to be  
728 supported by loop if the TSS of it was lying in one loop anchor while enhancer in the other. Correlation  
729 analysis was performed based on the usage of updated InTAD package<sup>49</sup> v1.9.2.

730

### 731 **Gene expression analysis**

732 The global ependymoma tumor gene expression data integration was performed based on the usage of  
733 corresponding R2 platform materials with focus on Affymetrix dataset from combined ependymoma  
734 tumors cohort with integration of normal brain tissues (n=618). Major of these ependymoma tumor  
735 Affymetrix materials were obtained from the corresponding main study<sup>1</sup> (GEO: GSE64415) with  
736 additional external inclusions (GEO: GSE50161, GSE50385, GSE21687, GSE3526). The gene  
737 ontology analysis was performed using DAVID tool<sup>50</sup> based on the usage of differentially expressed  
738 genes between PFA and other ependymoma groups achieved with R2 platform from the EPN global  
739 Affymetrix dataset. The RNA-sequencing materials from target EPN cohort samples were analyzed as  
740 previously described<sup>18</sup>.

741

#### 742 **Structural variants (SV) discovery from Hi-C data**

743 SV discovery from Hi-C data was performed using two independent toolkits. The first toolkit,  
744 hicBreakFinder ([https://github.com/dixonlab/hic\\_breakfinder](https://github.com/dixonlab/hic_breakfinder)), was adjusted for the usage on hg19  
745 human genome reference with taking into account additional filtering lists of false positives obtained  
746 from external cohorts<sup>19</sup>. Shortly, the tool scans for abrupt shifts in chromosomal connections in order  
747 to find possible outliers representing inter/intra-chromosomal events based on the selected threshold  
748 ( $t=0.6$ ) and reports them in resolutions 1Mb, 100Kb and 10Kb. Final combined result contains the  
749 highest resolution for detected SV. The second toolkit, Hi-C structural variant discovery or HiCsv,  
750 consists of two parts and was adjusted for the usage of hg38 genome as the most up-to-date reference  
751 genome. First part of this toolkit, HiCtrans<sup>21</sup>, focuses on inter-chromosomal translocations: it scans  
752 the inter-chromosomal contact matrices over multiple Hi-C resolutions for each possible pair of  
753 chromosomes from a given sample and predicts candidate SVs based on the changepoint analysis using  
754 binary segmentation. The intra-chromosomal translocations are also detected in this toolkit based on  
755 the dual pattern of off-diagonal enrichment and diagonal depletion of chromatin interactions in a Hi-  
756 C map across genomic regions. HiCsv detects enrichment of interactions through FitHiC2 algorithm<sup>45</sup>  
757 and uses an insulation score-based estimation (similar to TAD finding<sup>51</sup>) to identify depletion in  
758 interaction frequency. Finally, it applies a density-based clustering of enriched Hi-C interactions with  
759 high insulation scores to discover structural variants.

760

#### 761 **CTCF ChIP-sequencing**

762 ChIP-sequencing procedure was prepared and performed as previously described<sup>18</sup>. Shortly, ChIP  
763 flash-frozen for ependymoma tumours was performed using 5  $\mu$ g CTCF antibody per ChIP Active  
764 Motif. Enriched DNA was quantified and barcoded. Following library amplification, DNA fragments  
765 were sequenced using Illumina HiSeq 2000 100-bp paired-end sequencing.

766

### 767 **CTCF ChIP-seq data analysis**

768 Reads alignment was performed to hg19 reference with BWA v0.5.10<sup>52</sup>. Duplicate alignments were  
769 removed using Picard (<http://broadinstitute.github.io/picard>). Peak calling was performed using Macs  
770 v1.4<sup>53</sup>. Differential RELA peaks between EPN PFA and RELA were detected using DiffBind R  
771 package<sup>54</sup> with min adjusted p-value limit 0.05.

772

### 773 **Whole genome bisulfite sequencing (WGBS)**

774 WGBS procedure was prepared and performed as previously described<sup>55</sup>. Shortly, 5 µg of genomic  
775 DNA were sheared using a Covaris device. After adaptor ligation, DNA fragments were isolated and  
776 bisulphite converted using the EZ DNA Methylation kit (Zymo Research). PCR amplification of the  
777 fragments was performed followed by library aliquots pooling. Sequencing was performed Illumina  
778 HiSeq 2000 machine.

779

### 780 **WGBS data analysis**

781 Initial reads processing was performed using methylTools v0.9.4 as previously described<sup>55</sup>.  
782 Differentially methylated regions were detected using methylKit v0.2.6 tool<sup>56</sup> with min adjusted p-  
783 value limit 0.05. Combined visualization of the methylation profiles within CTCF target regions was  
784 performed using the EnrichedHeatmap R package. Search of target loops was performed based on the  
785 presence of overlapping the DMRs with differential CTCF peaks within.

786

### 787 **Cell culture**

788 HEK293T cells (CRL-1273, American Type Culture Collection) were cultured as previously described  
789 (citation). EPD210FH cells were grown in NeuroCult NS-A Basal Medium (STEMCELL  
790 Technologies) supplemented with NeuroCult Proliferation Supplement (STEMCELL Technologies),  
791 2mM L-glutamine 1% Penicillin/Streptomycin, 75ng/ml bovine serum albumin (BSA) and 20ng/ml of  
792 EGF (PeproTech) and FGF-basic (PeproTech). EP1NS cells were grown in Neurobasalmedium A (Life  
793 Technologies) supplemented with 1µg/ml of Heparin (Sigma), 2mM L-Glutamine and 20ng/ml of EGF  
794 and FGF-basic. Cells were cultured as neurospheres in tissue culture flasks. When they were cultured  
795 as an adherent culture, flask was additionally coated with Laminin (L2020, Sigma) for EPD210FH  
796 cells and with Geltrex (A1569601, Life Technologies) for EP1NS cells. Pediatric patient-derived SU-  
797 pcGBM2 cells were cultivated as neurospheres as previously described. (Katrin Schramm paper,  
798 2019). All cells were routinely tested free of mycoplasma contamination and authenticated by Single

799 Nucleotide Polymorphism profiling (Multiplexion GmbH). All cell models were grown at 37°C with  
800 5% CO<sub>2</sub>.

801

### 802 **Lentiviral Transduction**

803 shRNA plasmids and sgRNA plasmids were constructed as previously described (STK3 paper). All  
804 oligos are ordered from Sigma. Target sequences of all oligos are listed in Supplementary Table S8.  
805 Transduction was performed in the presence of protamine sulfate (final concentration 5 ug/mL, Sigma-  
806 Aldrich) Transduced cells were further cultured and GFP signal was analyzed by BD FACS Canto for  
807 GFP expression. Reduction of the percentage of GFP-positive cells indicates that the infected cells  
808 expressing a particular shRNA/ sgRNA have a growth disadvantage in comparison to the non-infected  
809 cells.

810

### 811 **Drug treatments**

812 All drugs were prepared according to protocols provided by company (Supplementary Table S9) Cells  
813 were seeded into 96-well cell culture treated plates at a density of 5000 cells in 100 µl respected  
814 medium per well. On the next day morning, cells were treated with increasing concentrations (200 nM,  
815 400 nM, 800 nM, 1.6 µM, 3.2 µM, 6.4 µM and 12.8 µM) of each drug or equivalent dilutions of  
816 solvent. Cell viability was assessed after 72 hours using the CellTiter-Glo<sup>®</sup> luminescent cell viability  
817 assay (Promega) and an automated plate reader Mythras. All samples were assayed in triplicates and  
818 normalized to the average values of the corresponding mock control on the same plate and analyzed  
819 using Prism 8 (GraphPad).

820

### 821 **Western blot analysis**

822 For knockdown and/or knockout studies, cells were infected as described above and cultured for either  
823 4 days (knockdown) or 5 days (knockout). Before harvesting, cells were washed with phosphate  
824 buffered saline (PBS) and collected as pellets. Then, pellets were lysed in RIPA buffer (Sigma-  
825 Aldrich) supplemented with protease and phosphatase inhibitors for 30 minutes on ice. After  
826 centrifugation at 13,000 rpm for 10 minutes at 4 °C, the supernatants were collected and protein  
827 concentrations were determined using a Bicinchoninic acid (BCA) assay (Sigma-Aldrich) with  
828 Pierce<sup>™</sup> bovine serum albumin standards (Thermo Fisher). Lysates were mixed with NuPAGE<sup>®</sup>  
829 LSD Sample buffer (Life Technologies) supplemented with 10 % 2-mercaptoethanol and denatured  
830 for 5 minutes at 95 °C. Afterwards they were subjected to sodium dodecyl sulfate-polyacrylamide gel  
831 electrophoresis according to standard procedures using 4-12 % Bis-Tris gels and afterwards transferred  
832 to polyvinylidene difluoride membranes. Membranes were incubated with respective primary

833 antibodies at 4 °C overnight (Supplementary Table S10). Horseradish peroxidase-conjugated anti-  
834 rabbit (1:5,000, Santa Cruz, sc-2054) secondary antibody were applied for 1 hour at room temperature  
835 and chemiluminescent detection was carried out using Amersham™ ECL™ or ECL™ Prime  
836 Western Blotting detection reagents (GE Healthcare). The same membranes were stripped with  
837 stripping buffer (Sigma) according to protocol and incubated with conjugated beta-actin antibody as a  
838 loading control.

839

#### 840 Data availability

841 The novel sequencing data raw materials (HiC, CTCF, WGBS) will be included into the European  
842 Genome-phenome archive (<https://www.ebi.ac.uk/ega/home>) under the accession number:  
843 GAS00001002696; this source already contains other data types (RNA-seq, H3K27ac) for the  
844 corresponding target tumor samples.

845

#### 846 Code availability

847 Scripts for processing the raw data and generating figures can be obtained upon request.

848

## 849 References

- 850 1 Pajtler, K. W. *et al.* Molecular Classification of Ependymal Tumors across All CNS  
851 Compartments, Histopathological Grades, and Age Groups. *Cancer Cell* **27**, 728-743,  
852 doi:10.1016/j.ccell.2015.04.002 (2015).
- 853 2 Pui, C. H., Gajjar, A. J., Kane, J. R., Qaddoumi, I. A. & Pappo, A. S. Challenging issues in  
854 pediatric oncology. *Nat Rev Clin Oncol* **8**, 540-549, doi:10.1038/nrclinonc.2011.95 (2011).
- 855 3 Siegel, R. L., Miller, K. D. & Jemal, A. Cancer statistics, 2016. *CA Cancer J Clin* **66**, 7-30,  
856 doi:10.3322/caac.21332 (2016).
- 857 4 Downing, J. R. *et al.* The Pediatric Cancer Genome Project. *Nat Genet* **44**, 619-622,  
858 doi:10.1038/ng.2287 (2012).
- 859 5 Mack, S. C. *et al.* Epigenomic alterations define lethal CIMP-positive ependymomas of  
860 infancy. *Nature* **506**, 445-450, doi:10.1038/nature13108 (2014).
- 861 6 Witt, H. *et al.* Delineation of two clinically and molecularly distinct subgroups of posterior  
862 fossa ependymoma. *Cancer Cell* **20**, 143-157, doi:10.1016/j.ccr.2011.07.007 (2011).
- 863 7 Parker, M. *et al.* C11orf95-RELA fusions drive oncogenic NF-kappaB signalling in  
864 ependymoma. *Nature* **506**, 451-455, doi:10.1038/nature13109 (2014).

- 865 8 Pajtler, K. W. *et al.* YAP1 subgroup supratentorial ependymoma requires TEAD and nuclear  
866 factor I-mediated transcriptional programmes for tumorigenesis. *Nature communications* **10**,  
867 1-16 (2019).
- 868 9 Panwalkar, P. *et al.* Immunohistochemical analysis of H3K27me3 demonstrates global  
869 reduction in group-A childhood posterior fossa ependymoma and is a powerful predictor of  
870 outcome. *Acta Neuropathol* **134**, 705-714, doi:10.1007/s00401-017-1752-4 (2017).
- 871 10 Pajtler, K. W. *et al.* Molecular heterogeneity and CXorf67 alterations in posterior fossa group  
872 A (PFA) ependymomas. *Acta Neuropathol* **136**, 211-226, doi:10.1007/s00401-018-1877-0  
873 (2018).
- 874 11 Hubner, J. M. *et al.* EZHIP / CXorf67 mimics K27M mutated oncohistones and functions as  
875 an intrinsic inhibitor of PRC2 function in aggressive posterior fossa ependymoma. *Neuro*  
876 *Oncol*, doi:10.1093/neuonc/noz058 (2019).
- 877 12 Araki, A. *et al.* Chromosome 1q gain and tenascin-C expression are candidate markers to  
878 define different risk groups in pediatric posterior fossa ependymoma. *Acta neuropathologica*  
879 *communications* **4**, 88 (2016).
- 880 13 Grubert, F. *et al.* Landscape of cohesin-mediated chromatin loops in the human genome.  
881 *Nature* **583**, 737-743 (2020).
- 882 14 Rhie, S. K. *et al.* A high-resolution 3D epigenomic map reveals insights into the creation of  
883 the prostate cancer transcriptome. *Nature communications* **10**, 1-12 (2019).
- 884 15 Kloetgen, A. *et al.* Three-dimensional chromatin landscapes in T cell acute lymphoblastic  
885 leukemia. *Nature Genetics* **52**, 388-400 (2020).
- 886 16 Li, Y., Hu, M. & Shen, Y. Gene regulation in the 3D genome. *Hum Mol Genet* **27**, R228-  
887 R233, doi:10.1093/hmg/ddy164 (2018).
- 888 17 Capper, D. *et al.* DNA methylation-based classification of central nervous system tumours.  
889 *Nature* **555**, 469-474 (2018).
- 890 18 Mack, S. C. *et al.* Therapeutic targeting of ependymoma as informed by oncogenic enhancer  
891 profiling. *Nature* **553**, 101-105, doi:10.1038/nature25169 (2018).
- 892 19 Dixon, J. R. *et al.* Integrative detection and analysis of structural variation in cancer genomes.  
893 *Nat Genet* **50**, 1388-1398, doi:10.1038/s41588-018-0195-8 (2018).
- 894 20 Lupianez, D. G. *et al.* Disruptions of topological chromatin domains cause pathogenic  
895 rewiring of gene-enhancer interactions. *Cell* **161**, 1012-1025, doi:10.1016/j.cell.2015.04.004  
896 (2015).
- 897 21 Chakraborty, A. & Ay, F. Identification of copy number variations and translocations in  
898 cancer cells from Hi-C data. *Bioinformatics* **34**, 338-345 (2018).

- 899 22 Wang, Y. *et al.* LSD1 co-repressor Rcor2 orchestrates neurogenesis in the developing mouse  
900 brain. *Nature communications* **7**, 10481, doi:10.1038/ncomms10481 (2016).
- 901 23 Maes, T. *et al.* ORY-1001, a potent and selective covalent KDM1A inhibitor, for the  
902 treatment of acute leukemia. *Cancer Cell* **33**, 495-511. e412 (2018).
- 903 24 Rajarajan, P. *et al.* Neuron-specific signatures in the chromosomal connectome associated  
904 with schizophrenia risk. *Science (New York, N.Y.)* **362**, doi:10.1126/science.aat4311 (2018).
- 905 25 Davis, C. A. *et al.* The Encyclopedia of DNA elements (ENCODE): data portal update.  
906 *Nucleic acids research* **46**, D794-D801, doi:10.1093/nar/gkx1081 (2018).
- 907 26 Michealraj, K. A. *et al.* Metabolic Regulation of the Epigenome Drives Lethal Infantile  
908 Ependymoma. *Cell*, doi:10.1016/j.cell.2020.04.047 (2020).
- 909 27 MacLeod, G. *et al.* Genome-Wide CRISPR-Cas9 Screens Expose Genetic Vulnerabilities and  
910 Mechanisms of Temozolomide Sensitivity in Glioblastoma Stem Cells. *Cell Rep* **27**, 971-986  
911 e979, doi:10.1016/j.celrep.2019.03.047 (2019).
- 912 28 Flavahan, W. A. *et al.* Insulator dysfunction and oncogene activation in IDH mutant gliomas.  
913 *Nature* **529**, 110-114, doi:10.1038/nature16490 (2016).
- 914 29 Flavahan, W. A. *et al.* Altered chromosomal topology drives oncogenic programs in SDH-  
915 deficient GISTs. *Nature* **575**, 229-233, doi:10.1038/s41586-019-1668-3 (2019).
- 916 30 Fujii, S., Matsumoto, S., Nojima, S., Morii, E. & Kikuchi, A. Arl4c expression in colorectal  
917 and lung cancers promotes tumorigenesis and may represent a novel therapeutic target.  
918 *Oncogene* **34**, 4834-4844, doi:10.1038/onc.2014.402 (2015).
- 919 31 Takagi, S. *et al.* LSD1 inhibitor T-3775440 inhibits SCLC cell proliferation by disrupting  
920 LSD1 interactions with SNAG domain proteins INSM1 and GFI1B. *Cancer Research* **77**,  
921 4652-4662 (2017).
- 922 32 Milde, T. *et al.* A novel human high-risk ependymoma stem cell model reveals the  
923 differentiation-inducing potential of the histone deacetylase inhibitor Vorinostat. *Acta*  
924 *neuropathologica* **122**, 637 (2011).
- 925 33 Park, D. E. *et al.* Merkel cell polyomavirus activates LSD1-mediated blockade of non-  
926 canonical BAF to regulate transformation and tumorigenesis. *Nature Cell Biology* **22**, 603-  
927 615 (2020).
- 928 34 Lathia, J. D. *et al.* Integrin alpha 6 regulates glioblastoma stem cells. *Cell Stem Cell* **6**, 421-  
929 432, doi:10.1016/j.stem.2010.02.018 (2010).
- 930 35 Martin, T. A. & Jiang, W. G. Evaluation of the expression of stem cell markers in human  
931 breast cancer reveals a correlation with clinical progression and metastatic disease in ductal  
932 carcinoma. *Oncol Rep* **31**, 262-272, doi:10.3892/or.2013.2813 (2014).

- 933 36 Hoogland, A. M. *et al.* Validation of stem cell markers in clinical prostate cancer: alpha6-  
934 integrin is predictive for non-aggressive disease. *Prostate* **74**, 488-496,  
935 doi:10.1002/pros.22768 (2014).
- 936 37 Schober, M. & Fuchs, E. Tumor-initiating stem cells of squamous cell carcinomas and their  
937 control by TGF-beta and integrin/focal adhesion kinase (FAK) signaling. *Proceedings of the*  
938 *National Academy of Sciences of the United States of America* **108**, 10544-10549,  
939 doi:10.1073/pnas.1107807108 (2011).
- 940 38 Haraguchi, N. *et al.* CD49f-positive cell population efficiently enriches colon cancer-  
941 initiating cells. *Int J Oncol* **43**, 425-430, doi:10.3892/ijo.2013.1955 (2013).
- 942 39 Zhang, Y. *et al.* Overexpression of LAMC1 predicts poor prognosis and enhances tumor cell  
943 invasion and migration in hepatocellular carcinoma. *J Cancer* **8**, 2992-3000,  
944 doi:10.7150/jca.21038 (2017).
- 945 40 Consortium, E. P. An integrated encyclopedia of DNA elements in the human genome.  
946 *Nature* **489**, 57-74 (2012).
- 947 41 Schmitt, A. D. *et al.* A compendium of chromatin contact maps reveals spatially active  
948 regions in the human genome. *Cell reports* **17**, 2042-2059 (2016).
- 949 42 Rao, S. S. *et al.* A 3D map of the human genome at kilobase resolution reveals principles of  
950 chromatin looping. *Cell* **159**, 1665-1680 (2014).
- 951 43 Servant, N. *et al.* HiC-Pro: an optimized and flexible pipeline for Hi-C data processing.  
952 *Genome biology* **16**, 259 (2015).
- 953 44 Durand, N. C. *et al.* Juicebox provides a visualization system for Hi-C contact maps with  
954 unlimited zoom. *Cell systems* **3**, 99-101 (2016).
- 955 45 Kaul, A., Bhattacharyya, S. & Ay, F. Identifying statistically significant chromatin contacts  
956 from Hi-C data with FitHiC2. *Nature Protocols* **15**, 991-1012 (2020).
- 957 46 Shin, H. *et al.* TopDom: an efficient and deterministic method for identifying topological  
958 domains in genomes. *Nucleic acids research* **44**, e70-e70 (2016).
- 959 47 Durand, N. C. *et al.* Juicer Provides a One-Click System for Analyzing Loop-Resolution Hi-  
960 C Experiments. *Cell systems* **3**, 95-98, doi:10.1016/j.cels.2016.07.002 (2016).
- 961 48 Lieberman-Aiden, E. *et al.* Comprehensive mapping of long-range interactions reveals  
962 folding principles of the human genome. *Science (New York, N.Y.)* **326**, 289-293,  
963 doi:10.1126/science.1181369 (2009).
- 964 49 Okonechnikov, K., Erkek, S., Korbil, J. O., Pfister, S. M. & Chavez, L. InTAD: chromosome  
965 conformation guided analysis of enhancer target genes. *BMC bioinformatics* **20**, 60 (2019).



966 50 Sherman, B. T. & Lempicki, R. A. Systematic and integrative analysis of large gene lists  
967 using DAVID bioinformatics resources. *Nature protocols* **4**, 44 (2009).

968 51 Dixon, J. R. *et al.* Topological domains in mammalian genomes identified by analysis of  
969 chromatin interactions. *Nature* **485**, 376-380 (2012).

970 52 Li, H. & Durbin, R. Fast and accurate short read alignment with Burrows–Wheeler transform.  
971 *bioinformatics* **25**, 1754-1760 (2009).

972 53 Zhang, Y. *et al.* Model-based analysis of ChIP-Seq (MACS). *Genome biology* **9**, 1-9 (2008).

973 54 Ross-Innes, C. S. *et al.* Differential oestrogen receptor binding is associated with clinical  
974 outcome in breast cancer. *Nature* **481**, 389-393 (2012).

975 55 Hovestadt, V. *et al.* Decoding the regulatory landscape of medulloblastoma using DNA  
976 methylation sequencing. *Nature* **510**, 537-541 (2014).

977 56 Jühling, F. *et al.* metilene: Fast and sensitive calling of differentially methylated regions from  
978 bisulfite sequencing data. *Genome research* **26**, 256-262 (2016).

979



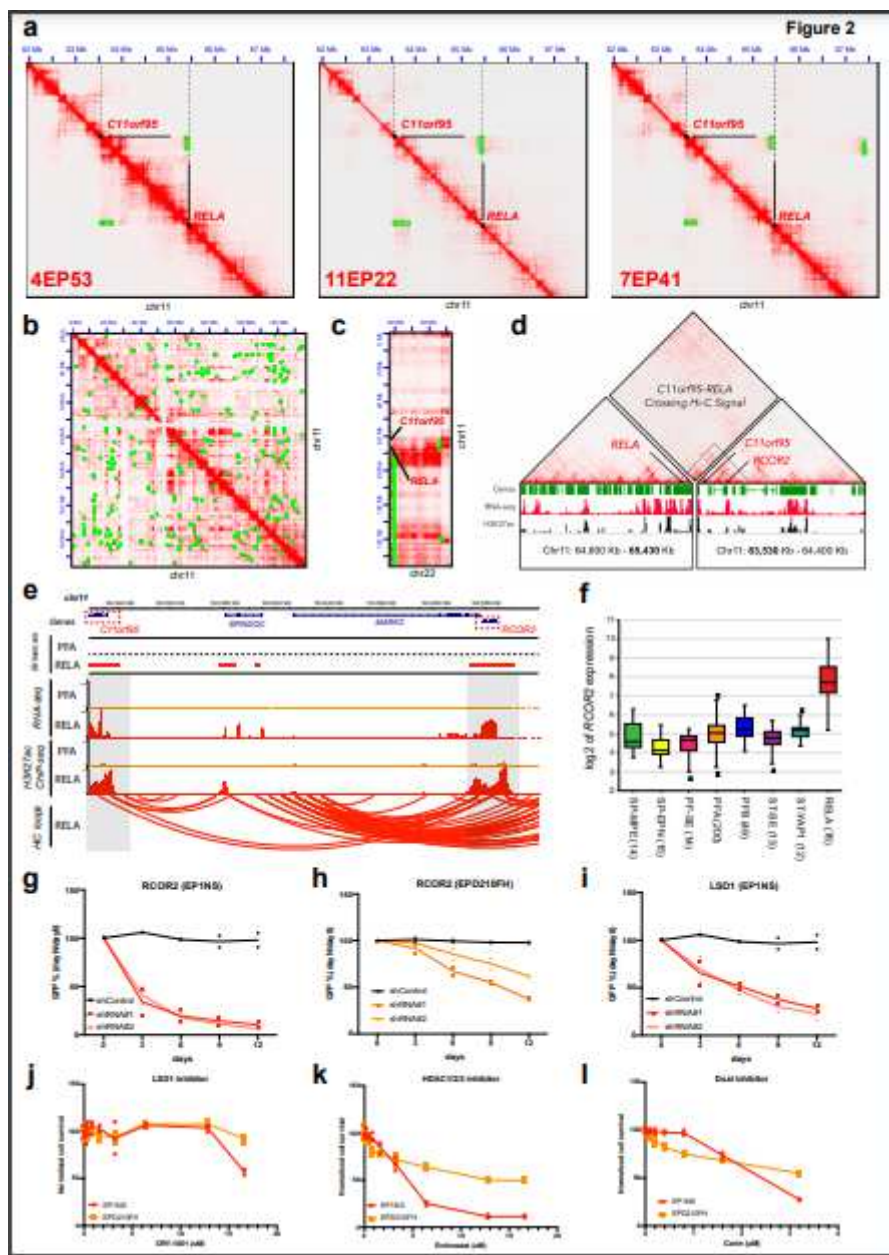


**Figure 2**

[Please see the manuscript file to view the figure caption.]

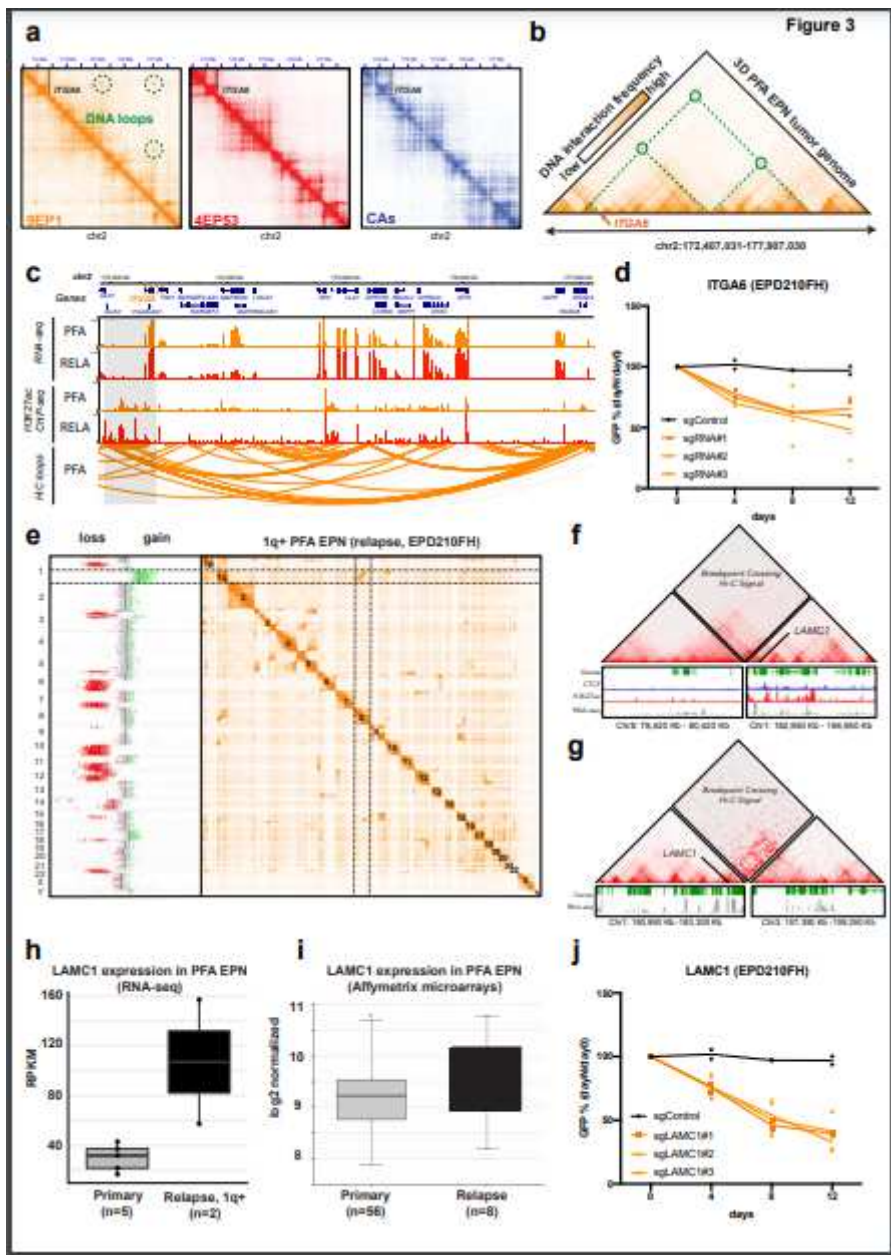


Figure 3

[Please see the manuscript file to view the figure caption.]

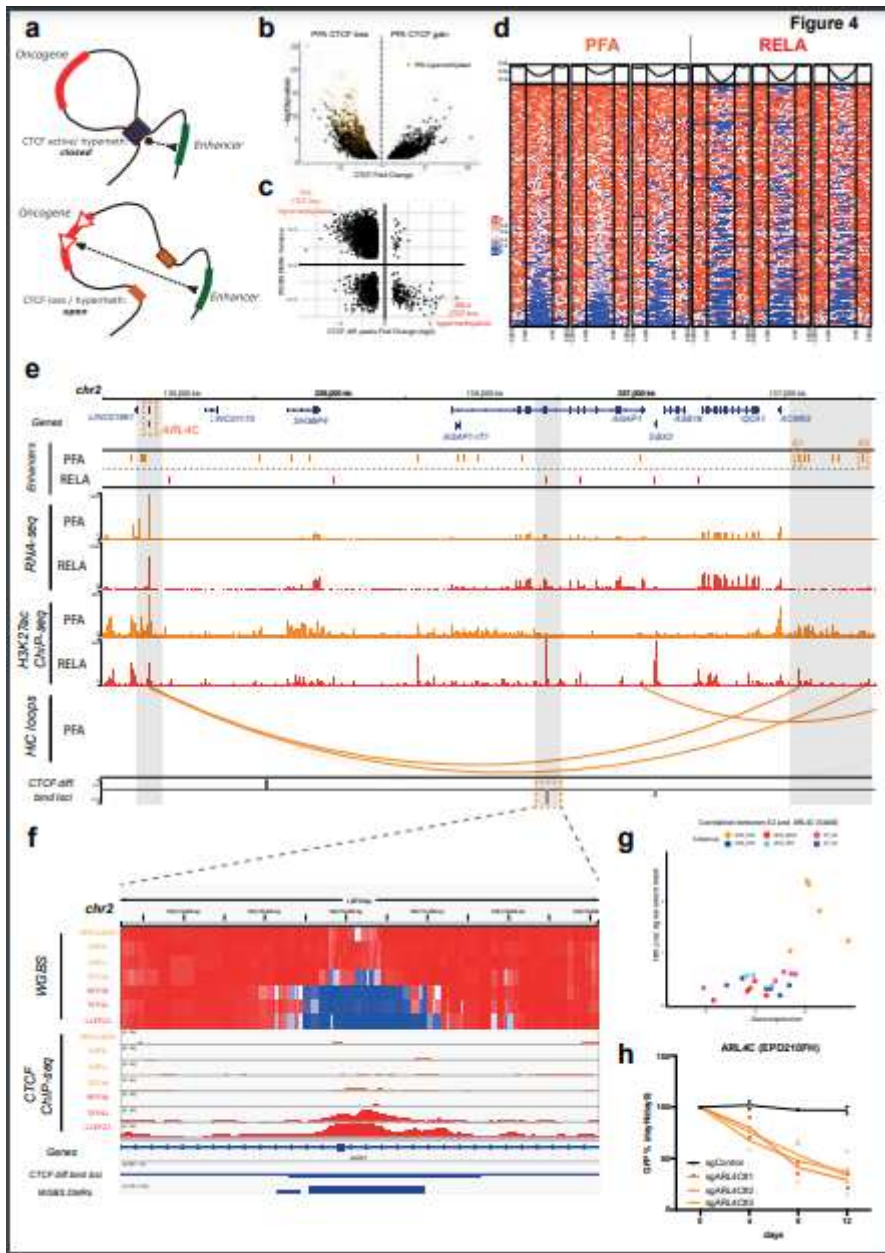


Figure 4

[Please see the manuscript file to view the figure caption.]

## Supplementary Files

This is a list of supplementary files associated with this preprint. Click to download.

- [EPNHiCtables.011020.xlsx](#)
- [SuppFigure1041020.pdf](#)
- [SuppFigure2041020.pdf](#)
- [SuppFigure3041020.pdf](#)
- [SuppFigure4041020.pdf](#)